by previous microstructure measurements. Despite its short duration, this episode was sufficient to boost daily-averaged turbulent eddy diffusivities in Saanich Inlet by two to three orders of magnitude. Daily-averaged diffusivities are 0.02×10^{-4} m^2 s^{-1} when dusk and dawn enhancement are excluded but 4×10^{-4} m^2 s^{-1} to 40×10^{-4} m^2 s^{-1} when they are included.

On a second day of sampling, the sky was overcast. At dusk, the backscattering layer began to migrate, though slightly later than the previous evening. Unlike the first evening, no discernible enhancement of turbulence was observed in the microstructure data. The acoustic data suggest that, for reasons unknown, the lower portion of the backscattering layer (the part most likely composed of the largest euphausiids) remained at depth. We hypothesize that larger euphausiids did not migrate, so that little or no turbulence was generated on the second night.

Several key groups of marine organisms, ranging from krill, to small pelagics such as herring and anchovies, to tuna, occur in sufficient abundance and in sufficiently dense schools to contribute substantial turbulent mixing, particularly in coastal waters (*10*). Our results confirm this for euphausiids in Saanich Inlet. The measured dissipation rates on the order of 10^{-5} W kg^{-1} are consistent with levels predicted for the Antarctic krill *E. superba* (*10*).

These data raise the possibility that a potentially important source of mixing in biologically productive parts of the upper ocean has been overlooked. Further data collected during June 2006 confirm the major results (*25*). Because many densely schooling species, particularly strong vertical migrators, are active near the base of the mixed layer, episodic biologically enhanced turbulence deserves further attention.

References and Notes

1. M. C. Gregg, *J. Geophys. Res.* **92**, 5249 (1987).
2. J. R. Ledwell, A. J. Watson, C. S. Law, *Nature* **364**, 701 (1993).
3. R. C. Hamme, S. R. Emerson, *J. Mar. Res.* **64**, 73 (2006).
4. W. Jenkins, S. Doney, *Global Biogeochem. Cycles* **17**, article no. 1110 (2003).
5. S. Vogel, *Life in Moving Fluids: The Physical Biology of Flow* (Princeton Univ. Press, Princeton, NJ, 1981).
6. U. Müller, B. van den Heuvel, E. Stamhuis, J. Videler, *J. Exp. Biol.* **200**, 2893 (1997).
7. J. Y. Cheng, G. Chahine, *Comp. Biochem. Physiol. A* **131**, 51 (2001).
8. J. Videler, E. Stamhuis, U. Müller, L. van Duren, *Integr. Comp. Biol.* **45**, 988 (2002).
9. W. Munk, *Deep-Sea Res.* **13**, 707 (1966).
10. M. E. Huntley, M. Zhou, *Mar. Ecol. Prog. Ser.* **273**, 65 (2004).
11. W. K. Dewar *et al.*, *J. Mar. Res.* **64**, 541 (2006).
12. R. K. Dewey, W. R. Crawford, *J. Phys. Oceanogr.* **18**, 1161 (1988).
13. A. S. Brierley *et al.*, *Limno. Oceanogr. Methods* **4**, 18 (2006).
14. A. E. Gargett, D. Stucchi, F. Whitney, *Estuar. Coast. Shelf Sci.* **56**, 1141 (2003).
15. C. F. Greenlaw, *Limnol. Oceanogr.* **24**, 226 (1979).
16. G. O. Mackie, C. E. Mills, *Can. J. Fish. Aquat. Sci.* **40**, 763 (1983).
17. M. Mangel, S. Nicol, *Can. J. Fish. Aquat. Sci.* **57** (suppl. 3), 1 (2000).
18. J. S. Jaffe, M. D. Ohman, A. De Robertis, *Can. J. Fish. Aquat. Sci.* **56**, 2000 (1999).
19. A. De Robertis, J. S. Jaffe, M. D. Ohman, *Limnol. Oceanogr.* **45**, 1838 (2000).
20. J. Yen, J. Brown, D. R. Webster, *Mar. Fresh. Behav. Physiol.* **36**, 307 (2003).
21. A. De Robertis, C. Schell, J. S. Jaffe, *J. Mar. Sci.* **60**, 885 (2003).
22. O. Yamamura, I. Inada, K. Shimazaki, *Mar. Biol.* **132**, 195 (1998).
23. A. De Robertis, *Limnol. Oceanogr.* **47**, 925 (2002).
24. A. E. Gargett, *J. Atmos. Oceanic Tech* **16**, 1973 (1999).
25. Measurements spanning three dusks and two dawns during 10 to 12 June 2006 found no discernible enhancement at the first dusk after an overcast day. After the sunny second and third days, elevated dissipation rates associated with vertical migration of the acoustic backscattering layer were observed during both dusk and dawn.

26. Data were collected with help from K. Brown and the crew of the *R/V Strickland*. Valuable comments were provided by J. Nash, T. Miller, J. MacKinnon, L. St. Laurent, W. Dewar, B. Legget, and R. Campbell. This research was made possible by the British Columbia Knowledge Development Foundation, the Canada Foundation for Innovation, the National Sciences and Engineering Council of Canada, and funds available to E.K. under the Canada Research Chair program.

1 May 2006; accepted 26 July 2006
10.1126/science.1129378

Solid Ammonium Sulfate Aerosols as Ice Nuclei: A Pathway for Cirrus Cloud Formation

J. P. D. Abbatt,[1]* S. Benz,[2] D. J. Cziczo,[3] Z. Kanji,[1] U. Lohmann,[3] O. Möhler[2]

Laboratory measurements support a cirrus cloud formation pathway involving heterogeneous ice nucleation by solid ammonium sulfate aerosols. Ice formation occurs at low ice-saturation ratios consistent with the formation of continental cirrus and an interhemispheric asymmetry observed for cloud onset. In a climate model, this mechanism provides a widespread source of ice nuclei and leads to fewer but larger ice crystals as compared with a homogeneous freezing scenario. This reduces both the cloud albedo and the longwave heating by cirrus. With the global ammonia budget dominated by agricultural practices, this pathway might further couple anthropogenic activity to the climate system.

Accurate representation of cirrus clouds remains a challenge to climate modeling, in part because of an incomplete understanding of ice cloud formation mechanisms (*1*). Whereas ice formation studies have been performed at higher temperatures (*2*), only recently has the cold cirrus regime been addressed. This has led to a homogeneous freezing model where ice nucleates directly from the aerosol aqueous phase (*3*). Heterogeneous freezing occurs through selective nucleation onto a small fraction of the background particles (*2*) at lower ice-saturation ratios (S_{ice}) than with homogeneous freezing. Traditionally, it has been thought that good heterogeneous ice nuclei are insoluble solids, such as mineral dust (*2*). Recently, it has been shown in the laboratory that soluble species can also act as ice nuclei in both the immersion (*4*, *5*) and deposition modes (*6*). In the latter case, Shilling *et al*. (*6*) demonstrated that roughly 1 in 10^5 supramicrometer-sized particles of solid ammonium sulfate on a cold plate act as ice nuclei at low ice supersaturations, suggesting that this could be an important atmospheric process. Here, we report measurements of the onset for deposition ice formation on solid ammonium sulfate aerosol under experimental conditions similar to those in the cirrus regime, and we assess the impact of this new ice formation mechanism on past laboratory experiments, field observations, and global climate.

Measurements at Storm Peak, CO, implicate a role of ammoniated particles in selective ice nucleation at low S_{ice} (*7*). It was observed that between 10^{-4} and 10^{-5} of the particles were heterogeneous ice nuclei. Of this fraction, roughly 25% were not classified as conventional insoluble ice nuclei particles—i.e., they did not contain substantial levels of mineral dust, elemental carbon, metal, or fly ash. Instead, these ice nuclei were sulfates, with some degree of organics present. Although the degree of neutralization of the particles was not measured, continental sulfate aerosol likely contains a large amount of ammonium (*8*).

These observations of selective heterogeneous ice nucleation on continental sulfate particles are consistent with laboratory ice nucleation experiments. Figure 1 presents data for two aerosol types representative of sulfate aerosol endpoints. H_2SO_4 particles exist in remote settings away from

[1]Department of Chemistry, University of Toronto, Toronto, ON M5S 3H6, Canada. [2]Institute for Meteorology and Climate Research (IMK-AAF), Forschungszentrum Karlsruhe, Postfach 3640, 76021 Karlsruhe, Germany. [3]Institute for Atmospheric and Climate Science, ETH Zurich, 8092, Zurich, Switzerland.

*To whom correspondence should be addressed. E-mail: jabbatt@chem.utoronto.ca

dominant sources of ammonia such as livestock and nitrogen-based fertilizer (*9*). $(NH_4)_2SO_4$, a major component of continental aerosol, is formed by the uptake of ammonia by H_2SO_4.

Figure 1A shows data for the homogeneous ice formation of H_2SO_4. Figure 1B shows $(NH_4)_2SO_4$ data from recent experiments with solid particles and from older experiments that attempted to measure homogeneous freezing conditions. Because we sought to distinguish the freezing behavior of H_2SO_4 from that of $(NH_4)_2SO_4$, we plotted only the results from homogeneous freezing experiments in which both materials had been studied by the same experimental approach and research group (*10*). Ice formation has been analyzed by means of infrared (IR) interrogation of submicrometer-sized particles in flow tubes (*11*–*14*), optical observation of supermicrometer-sized particles on a hydrophobic support (*15*, *16*), calorimetry of emulsified samples (*16*), optical counting of particles exiting an ice nucleation chamber (*17*), and optical counting/Fourier transform infrared observation in a low-temperature, expansion cloud chamber (*18*, *19*).

H_2SO_4 freezing conditions show good agreement, validating all of the experimental techniques (Fig. 1A). The results match those of the homogeneous freezing model, supporting a homogeneous freezing mechanism for H_2SO_4. By contrast, the freezing conditions for $(NH_4)_2SO_4$ span a wide range (Fig. 1B). The recent experiments for heterogeneous freezing yield low S_{ice} onsets. The literature experiments attempting to measure homogeneous freezing result in a much wider range of freezing conditions.

The relationship between the ice onsets and the fraction of particles freezing provides insight into the wide variability. The experiments most sensitive to a small freezing fraction are the flow tube and cloud chamber (*11*, *13*, *18*, *19*), in which sensitivity is 1 in 10^3 to 10^5 particles—i.e., approximately the ice nuclei fraction exhibited in the field (*2*). This sensitivity arises in the flow tube from a Bergeron-like transfer of water from aqueous particles to a small number of frozen particles (*2*, *20*). By contrast, the hydrophobic support and emulsion experiments (*15*, *16*) measure lower freezing temperatures, in part because they report freezing of a large fraction of the particles and because they study orders of magnitude fewer particles. The results from the ice nucleation chamber indicate that the onset S_{ice} of $(NH_4)_2SO_4$ depends on the aerosol freezing fraction; onsets for 1% freezing were higher than those for 0.1% (Fig. 1B) (*17*).

Why do a select fraction of particles initiate ice formation with $(NH_4)_2SO_4$ but not H_2SO_4? Recent laboratory results indicate that solid $(NH_4)_2SO_4$ particles can act as deposition ice nuclei (Fig. 1B). In particular, under conditions that are similar to those in the atmosphere, we used a cloud chamber to observe ice onsets for both solid and liquid $(NH_4)_2SO_4$ particles. Solid particles that were formed by efflorescence at 295 K and less than 10% relative humidity (RH) nucleate ice efficiently: onset S_{ice} = 1.20 at 221 K. For aqueous particles, the onset is close to that for H_2SO_4: S_{ice} = 1.55 at 219 K. The onset becomes slightly lower and the fraction of deposition ice nuclei increases as aqueous particles are exposed to drier conditions before the ice formation phase of the experiment; that is, additional particles crystallized at the lower RH [supporting online material (SOM) text]. We also studied aqueous $(NH_4)_2SO_4$ particles sprayed onto a hydrophobic support. Ice has also been observed to form selectively at low supersaturations (Fig. 1B). Additional details on the experimental technique and preliminary results at 233 K are described in the SOM text and (*21*, *22*).

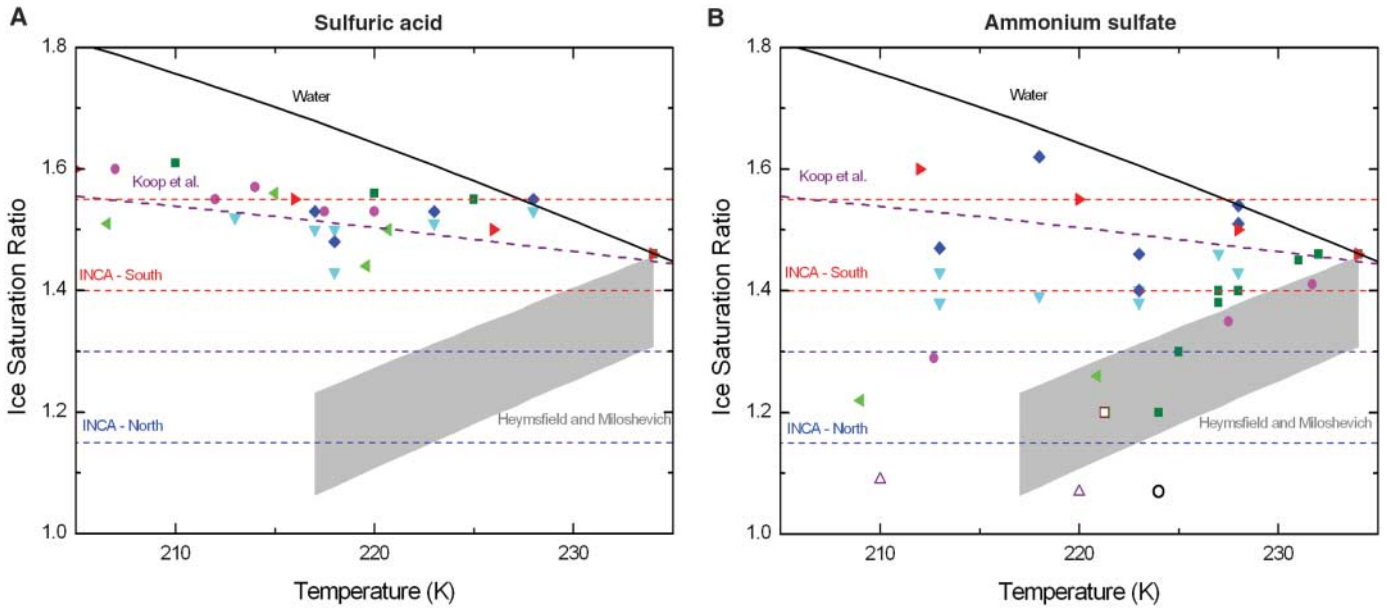

Fig. 1. (**A**) Ice formation points for sulfuric acid, plotted as saturation ratio with respect to ice as a function of temperature. Cziczo and Abbatt (*14*), flow tube/IR (dark green ■); Prenni *et al*. (*12*), flow tube/IR (pink ●); Koop *et al*. (*15*), hydrophobic support/optical (red ▶); Chen *et al*. (*17*), thermal-gradient diffusion chamber, data for 0.1% of the aerosol population freezing (light blue ▼); Chen *et al*. (*17*), thermal-gradient diffusion chamber, data for 1% of the aerosol population freezing (dark blue ◆); Möhler *et al*. (*18*), cloud chamber/IR/optical, data for the first run on each aerosol sample in Experiment Series B, and Mangold *et al*. (*19*), cloud chamber/IR/optical (light green ◀). Also shown are the liquid water saturation line [solid black line (fig. S1)]; water activity–based homogeneous freezing model of Koop *et al*. (*3*) (dashed purple line, nucleation rate = 10^{10} cm^{-3} s^{-1}); bounds for cirrus formation from Heymsfield and Miloshevich (*24*) (shaded gray area); upper and lower limits for cirrus formation in northern INCA campaign (dashed blue lines); and upper and lower limits for cirrus formation in southern INCA campaign (dashed red lines) (*26*). (**B**) Ice formation points for $(NH_4)_2SO_4$, plotted as supersaturation with respect to ice as a function of temperature. Solid symbols show data for homogeneous freezing conditions and open symbols show more recent data for solid particles. Cziczo and Abbatt (*13*), flow tube/IR (dark green ■); Wise *et al*. (*11*), flow tube/IR (pink ●); Bertram *et al*. (*16*), hydrophobic support/optical and emulsion/scanning calorimetry (red ▶); Chen *et al*. (*17*), thermal-gradient diffusion chamber, data for 0.1% of the aerosol population freezing, wet particles with preconditioner (light blue ▼); Chen *et al*. (*17*), thermal-gradient diffusion chamber, data for 1% of the aerosol population freezing (dark blue ◆); and Mangold *et al*. (*19*), cloud chamber/IR/optical, (light green ◀). Also plotted are onsets for heterogeneous ice nucleation by solid $(NH_4)_2SO_4$ as measured in our laboratories with particles deposited on a hydrophobic support (black ○) and in a large cloud chamber (brown □), and by Shilling *et al*. (*6*) (purple △). Additional new data from the cloud chamber are plotted in fig. S1. Solid and dashed lines and gray area are the same as in (**A**).

Deposition ice formation can explain some of the disparity between the published ice onsets in the experiments that sought to study homogeneous freezing of $(NH_4)_2SO_4$. Given that the particles in the flow tubes were sometimes briefly exposed to somewhat reduced RH when mixed into the carrier gas, a fraction may have effloresced at low temperature, thus driving ice nucleation heterogeneously. This finding is also in agreement with new results in which a polycrystalline sample with high surface area was seen to promote selective ice nucleation by deposition nucleation (*6*) but not with the earlier work of Chen *et al*. (*17*) (SOM text). $(NH_4)_2SO_4$ can be an efficient immersion ice nucleus (*4*, *23*). Overall, the findings that soluble species can act as ice nuclei challenge the traditional understanding in cloud physics that only insoluble species can act in this manner (*2*).

Some cirrus cloud formation observations are consistent with ammoniated sulfate particles acting as low-temperature ice nuclei. As noted previously (*14*), cirrus onsets measured in the field correspond with those from the flow tube for both ammonium sulfate and bisulfate. This is shown in Fig. 1B, where bounds for cirrus onset in one continental regime are indicated (*24*). The laboratory measurements sensitive to ice onset of 1 in 10^3 to 10^5 particles, in particular the cloud chamber work that is conducted under the most atmospherically relevant conditions, are similar to the field observations (Fig. 1A). Measurements in the North American free troposphere indicate that particles are neutralized to a large degree by ammonia (*8*). Given that the residence time for such particles can be long, individual particles within the same air volume experience different prior RH and temperatures. As shown by a trajectory modeling study (*25*), it is likely that a large fraction of the total sulfate aerosol will be exposed to RHs sufficiently low to induce efflorescence of solid ammoniated sulfates, particularly in the upper troposphere and Northern Hemisphere.

As a second example, the interhemispheric differences in cirrus properties from anthropogenic emissions (INCA) campaigns studied cirrus formation in clean air of oceanic origin in the Southern Hemisphere (centered at Punta Arenas, Chile, 54°S, March to April) and in moderately polluted air of mixed oceanic-continental origin in the Northern Hemisphere (centered at Prestwick, Scotland, 55°N, September to October). The ice cloud S_{ice} onsets were considerably different between the locations, occurring between 1.15 and 1.30 in the North and between 1.40 and 1.55 in the South (dashed lines in Fig. 1) (*26*). Given that the mean temperature of the measurements was 225 K (*27*), Fig. 1A demonstrates that the conditions for cirrus formation in the South are best matched by those for homogeneous freezing of H_2SO_4, whereas in Fig. 1B there is overlap between northern cirrus formation conditions and those for heterogeneous ice formation by means of $(NH_4)_2SO_4$.

The ammonium-to-sulfate molar ratio of the aerosol was not measured during INCA. However, measurements in the North Atlantic free troposphere indicate ratios that are sometimes close to 2 (*28*). In the Southern Hemisphere, where continental sources of ammonia are less important, the few measurements indicate values of 1 or lower (*29*, *30*). Models predict some difference in the degree of aerosol neutralization between the southern and northern INCA locations at the time of the campaigns (*9*, *31*, *32*). In particular, in the South (March to May), the aerosol is acidic, whereas in the North (September to November), it is more neutralized with compositions between $(NH_4)_2SO_4$ and NH_4NO_3 (*32*). Colberg *et al*. (*25*) predict that a major fraction of the Northern Hemispheric sulfate aerosol will contain solids, whereas liquids will prevail in the Southern Hemisphere.

Haag *et al*. (*27*) have analyzed the INCA data and concluded that a homogeneous freezing mechanism prevails in the South, whereas a coupled mechanism involving homogeneous freezing and selective heterogeneous freezing occurs in the North. However, these authors were not able to identify the chemical nature of the ice nuclei. Based on the laboratory evidence in Fig. 1 and the expected aerosol composition, we believe that cirrus formation occurred by homogeneous freezing of sulfuric acid particles in the southern INCA flights, whereas we raise the possibility that a fraction of ammoniated sulfate particles may have heterogeneously initiated cirrus formation at lower S_{ice} in the North.

As shown by the Storm Peak data, heterogeneous ice nucleation may proceed through a variety of ice nuclei, including mineral dust, metals, soot, solid organics, and, as demonstrated here, $(NH_4)_2SO_4$. Of these, fresh mineral dust is an especially efficient ice nucleus, likely much more efficient than $(NH_4)_2SO_4$ on a per surface area basis. However, there is considerably less mineral dust in the upper troposphere than there is sulfate aerosol, especially away from dust-source regions. Also, the dust can be coated heterogeneously with organics or sulfate, or it may be removed by the initial stages of cirrus formation. Conclusively evaluating the ice nuclei efficiency of $(NH_4)_2SO_4$ and other solid ammoniated sulfates relative to that of dust and other solids, in campaigns such as INCA or in the atmosphere in general, requires measurements of the degree of effloresced sulfate particles and the S_{ice} onset's dependence on particle surface area, mode of preparation (SOM text), and effects of other species present such as organics. In this context, the most atmospherically appropriate measurements we performed are those from the expansion cloud chamber, in which the particles effloresced homogeneously and low total surface areas were used.

To estimate the potential importance of ammoniated ice nuclei, we introduced ammonia into the ECHAM4 General Circulation Model (*22*, *33*). When heterogeneous freezing of either $(NH_4)_2SO_4$ or dust competes with homogeneous freezing, the number of ice crystals is reduced and the crystals grow larger. For $(NH_4)_2SO_4$, this reduces the shortwave cloud forcing (difference between all-sky and clear-sky radiation at the top of the atmosphere) for cirrus clouds between 0.5 and 0.9 W m^{-2}, as can be expected from parcel model studies (*34*) (Table 1). These bigger crystals sediment faster, reducing the ice water content and the longwave cloud forcing between 0.5 and 1.1 W m^{-2} (Table 1). Because the longwave effect partly offsets the shortwave effect, the net effect for $(NH_4)_2SO_4$ is a larger cooling by up to 0.3 W m^{-2} depending on the chosen scenario (SOM text). In the case of dust acting as ice nuclei, the net cooling can amount to 2.5 W m^{-2}, which emphasizes the importance of determining the relative efficiency of these two potential ice nuclei.

If crystalline ammoniated sulfate particles act as ice nuclei, biogeochemical processes that occur in continental regions are connected to ice cloud formation. Atmospheric ammonia has been highly anthropogenically affected, now being released primarily through livestock and nitrogen-based fertilizer, alongside smaller vegetation and oceanic and biomass burning sources (*9*). The impact of these agrarian practices on upper tropospheric ice clouds and climate has not been evaluated.

Table 1. Global annual mean shortwave, longwave, and net cloud forcing (difference between all-sky and clear-sky conditions) at the top of the atmosphere; ice water path; and vertically integrated ice crystal number concentration for the different model simulations. HOM: only homogeneous freezing; DU1 and DU10: heterogeneous freezing whenever the dust ice nuclei concentration exceeds 1 cm^{-3} or 0.1 cm^{-3}, respectively, and homogeneous freezing otherwise; AS1, AS10, and AS100: same categorization as DU1, but instead of dust, 1, 10, or 100% of the $(NH_4)_2SO_4$ concentration, respectively, serve as ice nuclei once the $(NH_4)_2SO_4$ number concentration exceeds 1 cm^{-3}.

	HOM	DU1	DU10	AS1	AS10	AS100
Shortwave cloud forcing (W m^{-2})	−48.2	−48.3	−47.0	−47.7	−47.7	−47.3
Longwave cloud forcing (W m^{-2})	29.5	29.3	25.8	29.0	28.7	28.4
Net cloud forcing (W m^{-2})	−18.7	−19.0	−21.2	−18.7	−19.0	−18.9
Ice water path (g m^{-2})	22.3	21.7	14.1	21.2	20.3	19.4
Ice crystal number (10^6 cm^{-2})	1.01	0.925	0.521	0.789	0.716	0.650

References and Notes

1. P. J. DeMott, in *Cirrus*, D. K. Lynch, Ed. (Oxford Univ. Press, New York, 2002), pp. 102–135.
2. H. R. Pruppacher, J. D. Klett, *Microphysics of Clouds and Precipitation* (D. Reidel, Dordrecht, Netherlands, 1984).
3. T. Koop, B. Luo, A. Tsias, T. Peter, *Nature* **406**, 611 (2000).
4. B. Zuberi, A. K. Bertram, T. Koop, L. T. Molina, M. J. Molina, *J. Phys. Chem. A* **105**, 6458 (2001).

5. B. Zobrist *et al.*, *Atmos. Chem. Phys. Discuss.* **6**, 3115 (2006).
6. J. E. Shilling, T. J. Fortin, M. A. Tolbert, *J. Geophys. Res.* **111**, D12204, 10.1029/2005JD006664 (2006).
7. P. J. DeMott *et al.*, *Proc. Natl. Acad. Sci. U.S.A.* **100**, 14655 (2003).
8. R. W. Talbot, J. E. Dibb, M. B. Loomis, *Geophys. Res. Lett.* **25**, 1367 (1998).
9. F. J. Dentener, P. J. Crutzen, *J. Atmos. Chem.* **19**, 331 (1994).
10. Other measurements in the literature are in general agreement with those presented in Fig. 1 or have been superseded by later measurements conducted by the same research group (*20*, *35*, *36*). In particular, the results of Chelf *et al.* (*36*) have been superseded by those of Hung *et al.* (*20*), which are in excellent agreement with those of Wise *et al.* (*11*) for the mean temperature of ice formation. Those of Prenni *et al.* (*12*) for ammonium sulfate have been superseded by those of Wise *et al.* (*11*).
11. M. E. Wise, R. M. Garland, M. A. Tolbert, *J. Geophys. Res.* **109**, D19203, 10.1029/2003JD004313 (2004).
12. A. J. Prenni, M. E. Wise, S. D. Brooks, M. A. Tolbert, *J. Geophys. Res.* **106**, 3037 (2001).
13. D. J. Cziczo, J. P. D. Abbatt, *J. Geophys. Res.* **104**, 13781 (1999).
14. D. J. Cziczo, J. P. D. Abbatt, *Geophys. Res. Lett.* **28**, 963 (2001).
15. T. Koop, H. P. Ng, L. T. Molina, M. J. Molina, *J. Phys. Chem. A* **102**, 8924 (1998).
16. A. K. Bertram, T. K. Koop, L. T. Molina, M. J. Molina, *J. Phys. Chem. A* **104**, 584 (2000).
17. Y. Chen, P. J. DeMott, S. M. Kreidenweis, D. C. Rogers, D. E. Sherman, *J. Atmos. Sci.* **57**, 3752 (2000).
18. O. Möhler *et al.*, *Atmos. Chem. Phys.* **3**, 211 (2003).
19. A. Mangold *et al.*, *Meteor. Zeitschr.* **14**, 485 (2005).
20. H.-M. Hung, A. Malinowski, S. T. Martin, *J. Phys. Chem. A* **106**, 293 (2002).
21. Z. Kanji, J. P. D. Abbatt, *J. Geophys. Res.*, **111**, D16204, 10.1029/2005JD006766 (2006).
22. Materials and methods are available as supporting material on *Science* Online.
23. A. Tabazadeh, O. B. Toon, *Geophys. Res. Lett.* **25**, 1379 (1998).
24. A. J. Heymsfield, L. M. Miloshevich, *J. Atmos. Sci.* **52**, 4302 (1995).
25. C. A. Colberg, B. P. Luo, H. Wernli, T. Koop, T. Peter, *Atmos. Chem. Phys.* **3**, 909 (2003).
26. J. Ström *et al.*, *Atmos. Chem. Phys.* **3**, 1807 (2003).
27. W. Haag *et al.*, *Atmos. Chem. Phys.* **3**, 1791 (2003).
28. J. E. Dibb, R. Talbot, E. M. Scheuer, *J. Geophys. Res.* **105**, 3709 (2000).
29. J. E. Dibb *et al.*, *J. Geophys. Res.* **101**, 1779 (1996).
30. B. J. Huebert *et al.*, *J. Geophys. Res.* **103**, 16493 (1998).
31. P. J. Adams, J. H. Seinfeld, D. M. Koch, *J. Geophys. Res.* **104**, 13791 (1999).
32. S. Martin *et al.*, *Atmos. Chem. Phys.* **4**, 183 (2004).
33. U. Lohmann, B. Kärcher, J. Hendricks, *J. Geophys. Res.* **109**, D16204, 10.1029/2003JD004443 (2004).
34. B. Kärcher, J. Hendricks, U. Lohmann, *J. Geophys. Res.* **111**, D01205, 10.1029/2005JD006219 (2006).
35. A. K. Bertram, D. D. Paterson, J. J. Sloan, *J. Phys. Chem.* **100**, 2376 (1996).
36. J. H. Chelf, S. T. Martin, *J. Geophys. Res.* **106**, 1215 (2001).
37. This work has been financially supported by the Natural Sciences and Engineering Research Council (Canada) and the Canadian Foundation for Climate and Atmospheric Sciences and by the European Union within the Integrated Project SCOUT-O3. We thank J. Shilling and M. Tolbert for sending a preprint of their work and anonymous reviewers and T. Koop for their comments.

Supporting Online Material

www.sciencemag.org/cgi/content/full/1129726/DC1
Materials and Methods
SOM Text
Figs. S1 to S3
References

9 May 2006; accepted 16 August 2006
Published online 31 August 2006;
10.1126/science.1129726
Include this information when citing this paper.

Global Genetic Change Tracks Global Climate Warming in *Drosophila subobscura*

Joan Balanyá,[1]* Josep M. Oller,[2] Raymond B. Huey,[3] George W. Gilchrist,[4] Luis Serra[1]

Comparisons of recent with historical samples of chromosome inversion frequencies provide opportunities to determine whether genetic change is tracking climate change in natural populations. We determined the magnitude and direction of shifts over time (24 years between samples on average) in chromosome inversion frequencies and in ambient temperature for populations of the fly *Drosophila subobscura* on three continents. In 22 of 26 populations, climates warmed over the intervals, and genotypes characteristic of low latitudes (warm climates) increased in frequency in 21 of those 22 populations. Thus, genetic change in this fly is tracking climate warming and is doing so globally.

Climate change is altering the geographic ranges, abundances, phenologies, and biotic interactions of organisms (*1*, *2*). Climate change may also alter the genetic composition of species, but assessment of such shifts requires genetic data sampled over time (*2*–*5*). For most species, time series of genetic data are nonexistent or rare, especially on continental or global scales (*5*). For a few *Drosophila* species, however, time-series comparisons of chromosomal inversions are feasible (*4*, *6*–*8*) because these adaptive polymorphisms were among the first genetic markers quantified in natural populations (*9*). Consequently, historical records of inversion frequencies in *Drosophila* spp. provide opportunities for evaluating genetic sensitivity to changes in climate and other environmental factors (*4*, *8*, *10*, *11*). Time-series data (13 to 46 years, mean = 24.1 years) of chromosomal-arrangement frequencies and of climate are now available for 26 populations of the cosmopolitan species *D. subobscura* on three continents. Here we examine whether ambient temperatures have warmed at these sites and also whether genotypes characteristic of low latitudes have increased in frequency.

Drosophila subobscura is native to the Old World, where it is geographically widespread from North Africa to Scandinavia (*12*). It has a rich complement of chromosomal arrangements (inversions) on its five acrocentric chromosomes (*12*). Over the past half-century, inversion frequencies have been scored at many sites in the Old World. The frequencies of most inversions change clinally with latitude and thus with climate (*13*, *14*). These climatic clines must be maintained dynamically by natural selection because the gene flow within continents is very high (*15*). Therefore, temporal shifts in inversion frequencies should be sensitive indicators of adaptive responses to climate change (*4*, *10*, *11*).

In the late 1970s, *D. subobscura* was accidentally introduced (*16*) into South America and soon thereafter (*17*) into North America. It spread explosively on both continents (*18*). Geneticists soon (1981 in South America, 1985 to 1986 in North America) began surveying inversion frequencies of these introduced populations at different latitudes (*19*, *20*). On both continents they detected incipient latitudinal clines in chromosome inversion frequencies that almost always had the same sign with latitude as in the Old World, supporting the inference that these clines are adaptive (*18*, *21*). Some other traits of these introduced flies show rapid clinal evolution as well (*22*, *23*).

To obtain comparative data on contemporary chromosome-arrangement frequencies, we and colleagues have revisited many of the historical sampling sites in both the Old and New World. Initial studies with *D. subobscura* reported that "warm-climate" inversions have increased in frequency at several European sites and proposed that these shifts reflect climate warming, but these studies did not investigate continent-scale correlations with climate (*10*, *11*, *24*, *25*). Our analyses here investigate whether the magnitude and direction of genetic shifts actually parallel those in climate, and whether they do so on all three continents.

[1]Department of Genetics, [2]Department of Statistics, Faculty of Biology, University of Barcelona, Diagonal 645, Barcelona 08071, Spain. [3]Department of Biology, Box 351800, University of Washington, Seattle, WA 98195–1800, USA. [4]Department of Biology, Box 8795, College of William and Mary, Williamsburg, VA 23187–8796, USA.

*To whom correspondence should be addressed. E-mail: jbalanya@ub.edu